Available online at www.sciencedirect.com

ScienceDirect

Physics Procedia 63 (2015) 85 – 90

Physics Procedia

43rd Annual Symposium of the Ultrasonic Industry Association, UIA Symposium 2014

Effects of ultrasound irradiation on the synthesis of metal oxide nanostructures

M. I. Díez-García[a], V. Manzi-Orezzoli[a], M. Jankulovska[a], S. Anandan[b], P. Bonete[a], R. Gómez[a], T. Lana-Villarreal[a]

[a]*Institut Universitari d'Electroquímica i Departament de Química Física, Universitat d'Alacant, Apartat 99, E-03080 Alacant (Spain)*
[b]*Nanomaterials and Solar Energy Conversion Lab, Department of Chemistry, National Institute of Technology, Trichy 620 015, India*

Abstract

High intensity ultrasound can be used for the production of novel nanomaterials, including metal oxides. According to previous works in this field, the most notable effects are consequence of acoustic cavitation. In this context, we have studied the preparation of different materials in the presence of ultrasound, including N-doped TiO_2 nanopowder, $NiTiO_3$ nanorods and MnO_x thin films. Ultrasound did not show a significant effect in all the cases. Exclusively for $NiTiO_3$ nanorods a reduction of the final particle size occurs upon ultrasonic irradiation. From these results, it can be concluded that the ultrasound irradiation does not always play a key role during the synthesis of metal oxides. The effects seem to be particularly relevant in those cases where mass transport is highly hindered and in those procedures that require the rupture of nanoparticle aggregates to obtain a homogenous dispersion.

Peer-review under responsibility of the Ultrasonic Industry Association

Keywords: Ultrasound-assisted synthesis; metal oxide nanostructures; N-doped TiO_2; $NiTiO_3$; MnO_x

1. Main Text

Research in nanoscience and nanotechnology fields has attracted tremendous attention in the last two decades. This has been promoted because the use of nanostructured materials has opened up new opportunities in different areas such as catalysis, energy production/storage, environmental protection, etc. In this context, the preparation of nanomaterials optimized for each application has become a real challenge. Among a variety of approaches, synthetic methods assisted by high intensity ultrasound irradiation have been described as promising routes to prepare these

Peer-review under responsibility of the Ultrasonic Industry Association
doi:10.1016/j.phpro.2015.03.014

nanomaterials without using bulk high temperatures and/or high pressures or long reaction times (Bang and Suslick, 2010, Gedanken, 2010, Geng, et al., 2012, Xu, et al., 2013).

The ultrasound irradiation (20 kHz-10 MHz) of a liquid can cause the effect known as acoustic cavitation. This is the main event in sonochemistry. It involves the generation, growth, and collapse of bubbles in the liquid. The bubble collapse induces extreme transient conditions such as the high temperatures (~ 5000 K) and pressures (~ 500 atm) that permit chemical reactions to occur (González-García, 2011). Most authors consider this process the main differential step in the ultrasonic assisted synthesis of nanomaterials (Bang and Suslick, 2010, Gedanken, 2010, Geng, et al., 2012, Xu, et al., 2013). In this regard, the generation of amorphous products is easily understood due to the very high cooling rates (in the ns time scale), which hinder atom organization, i.e. crystallization. However, the creation of well-defined nanostructures in the presence of ultrasound is not so well rationalized, although the volatile character of the solvent seems to play a key role. The possible physical effects caused by the ultrasound should also be mentioned. The most important ones are related to high-speed microjets and intense shock waves induced by cavitation.

In the last years, numerous works have appeared in the literature describing the ultrasound-assisted synthesis of a large variety of materials, both organic and inorganic. Among the latter, particular attention has been paid to the generation of metal nanoparticles, because it has the advantage, compared to traditional synthetic methods, that no chemical reducing agent is needed. Nevertheless, the methodology has also been applied to the preparation of other inorganic materials such as metal chalcogenides, carbides, and oxides. In almost all cases, the material (crystalline or amorphous) is in the nanometer size regime.

The use of ultrasound during the preparation of metal oxides has several advantages such as the possibility of obtaining either well-crystallized materials without using high temperatures or different nanoparticle morphologies. Even important changes in the composition of the final nanomaterial (doping) have been described. In this work, we address the sono(electro)chemical synthesis of several metal oxides that can be used in different environmental and solar energy harvesting devices. We have synthesized nanoparticles (N-doped TiO_2, $NiTiO_3$) by sonicating the precursor solution and thin films (MnO_x) combining ultrasound and electrochemical methods. The effect of ultrasound irradiation on the final nanostructure and composition is analyzed by TEM, SEM, UV-Vis spectroscopy, and cyclic voltammetry.

2. Materials and methods

2.1 Material synthesis

2.1.1. N-doped TiO_2

Nanocrystalline N-doped TiO_2 was prepared based on the synthesis of Wang et al. (Wang et al., 2011). Briefly, the procedure consists in dissolving 5.0 g of urea in 10 mL of deionized water + 10 ml of isopropyl alcohol. This solution was placed in an ice bath and subsequently, 30 mL of a mixture of titanium isopropoxide (TPT):isopropyl alcohol (v:v 1:2) was added dropwise. The reaction mixture was sonicated by direct immersion of a titanium horn (Ultrasonics vibracell, 20 kHz) for 150 min controlling the temperature at 70-80 ºC. The obtained powder was recovered by centrifugation and washed twice with water and ethanol (sample US-ND). For the undoped sample (US-UD), the procedure was repeated without adding urea to the reaction mixture. To study the effect of the ultrasonic field, the step involving sonication was substituted by mechanical stirring of the solution at 75 ºC. This procedure led to sample MS. For comparison, an N-doped TiO_2 sample was synthesized using the hydrothermal method reported by Wang et al. (Wang et al., 2009). In this route, a thermal treatment at 350 ºC for 4 h was required for the crystallization of the sample (ND-HM).

2.1.2. $NiTiO_3$

$NiTiO_3$ nanorods were prepared by the hydrothermal method described by Qu et al (Qu et al., 2012). In a typical synthesis, 2.48 g of nickel (II) acetate was dissolved in 60 mL of ethylene glycol. Afterwards, 3.4 mL of TPT was

added dropwise under stirring at room temperature. The resultant green suspension was stirred for 2 h at room temperature. The solution turned light blue. A precipitate of the same color was recovered by vacuum filtration, washed with ethanol several times, and dried under vacuum at 80 °C for 1 h. Finally, the powder was calcined at 600 °C for 2 h in air, obtaining the Hy-$NiTiO_3$ sample.

The sonochemical synthesis of $NiTiO_3$ nanorods was achieved using an adaptation of the previously described procedure. The TPT was added dropwise to the nickel (II) acetate/ethylene glycol solution under sonication (Ti-horn, 20 kHz), and the irradiation was continued until the suspension turned light blue. The following steps were identical, obtaining the $NiTiO_3$ nanorods named Sono-$NiTiO_3$.

$NiTiO_3$/FTO electrodes were prepared by doctor blading an aqueous slurry of the corresponding powders and subsequent thermal treatment at 600 ºC for 1 h. The film thickness was measured by an Alpha Step D-100 profilometer.

2.1.3. Manganese oxide films

Thin manganese oxide films were obtained by potentiodynamic electrodeposition by employing a modification of the procedure described by Gorlin and Jaramillo (Gorlin and Jaramillo, 2010). The deposition solution was prepared by dissolving 2.15 g of sodium sulfate and 3.7 g of manganous acetate in 150 mL of deionized water. The solution was aged until pH 7.1 was attained. Manganese oxide was deposited potentiodynamically by using a conducting glass substrate (FTO) as a working electrode. A Pt wire was used as a counter electrode and an Ag/AgCl/KCl (sat.) as a reference electrode. The electrodeposition on the FTO substrate was performed by cycling 9 times at a sweep rate of 20 mV s^{-1} between 0 V and 0.6 V vs. Ag/AgCl under magnetic stirring at 900 rpm. After deposition, the electrode was rinsed with deionized water and heated at 480 ºC for 10 h to obtain the Mn oxide/FTO electrode (sample MS-MnO_x).

The above-mentioned method was modified in order to investigate the effect of the presence of an ultrasonic field. Magnetic stirring was substituted by irradiation of low-frequency ultrasound (Ultrasonics Vibracel, 20 kHz) by immersing a titanium horn in the solution during electrodeposition. The MnO_x/FTO electrode thus obtained was called Sono-MnO_x.

2.2 Material characterization

Morphological characterization of the nanomaterials was carried out by transmission electron microscopy (TEM, JEM-2010 from JEOL) by field emission scanning electron microscopy (FE-SEM, MERLIN compact VP from Zeiss) or by scanning electron microscopy (SEM, JSM 840 from JEOL). A Shimadzu UV-2401PC spectrophotometer equipped with an integrating sphere was used to measure the UV-visible spectra.

(Photo)electrochemical measurements were performed at room temperature in a three-electrode cell equipped with a fused silica window. All potential were measured against and referred to an Ag/AgCl/KCl (sat.) electrode. Measurements were carried out with a computer-controlled Autolab PGSTAT30 potentiostat. When needed, a 1000 W Hg(Xe) arc lamp equipped with a water filter and a cutoff filter ($\lambda \geq 350$ nm, Newport model FSR-KG3) was used as a UV-visible light source. The applied light irradiance was 500 mW cm^{-2}

3. Results and discussions

3.1 Synthesis of visible light active N-doped TiO_2

Figure 1 shows TEM images of samples prepared using ultrasound (US-ND) and magnetic stirring (MS). In both cases, the as-generated powder is composed by extremely small nanoparticles in the range of 5 nm. No clear morphological differences are observed.

The introduction of ultrasound during the synthesis was expected to cause the decomposition of urea, generating nitrogen-doped TiO_2. However, no differences in the UV-visible diffuse reflectance spectra were observed for samples US-ND, US-UD and MS. Only the doped sample prepared by the hydrothermal method (ND-HM) shows a

red-shifted reflectance spectrum. To verify whether the decomposition of urea exclusively occurs at high frequencies, the synthesis was repeated using 863 kHz irradiation (Meinhardt Multifrequency), yielding sample US863. However, as revealed by the UV-visible spectrum no significant changes were observed in the resulting product.

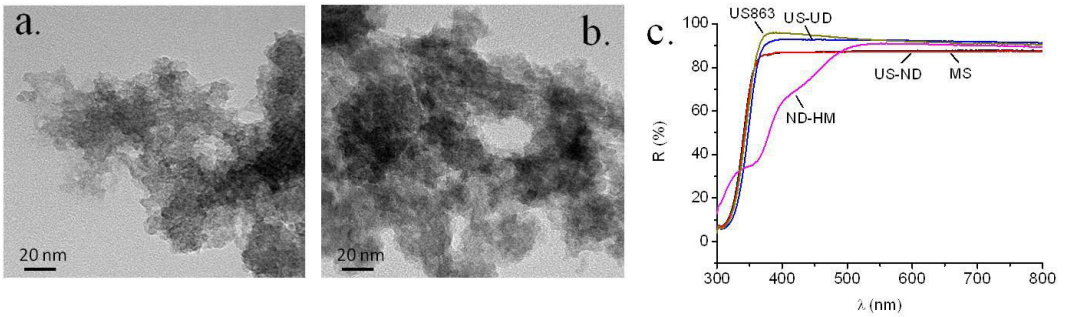

Fig. 1. TEM micrographs of US-ND (a) and MS (b) samples. UV-visible diffuse reflectance spectra for samples prepared under ultrasonic irradiation (US863, US-ND, US-UD), by magnetic stirring (MS), and hydrothermally (ND-HM).

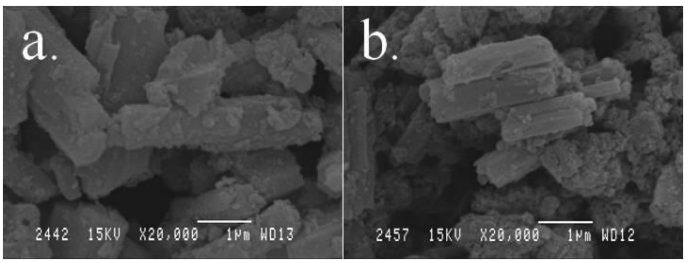

Fig 2. SEM micrographs of $NiTiO_3$/FTO electrodes based on (a) Hy-$NiTiO_3$ and (b) Sono-$NiTiO_3$ nanorods.

3.2 Synthesis of n-type $NiTiO_3$ nanorods

Independently if the synthesis of $NiTiO_3$ was carried out in the presence/absence of ultrasound, a nanopowder composed of well-crystallized $NiTiO_3$ (as revealed by XRD, not shown) was generated. A careful inspection by TEM (Figure 2) revealed that in both cases the sample is composed of nanorods, being slightly smaller those prepared by ultrasound-assisted synthesis (Sono-$NiTiO_3$). Concretely, the nanorods of Sono-TiO_3 are 1,8 ± 0,5 µm in length and 0,6 ± 0,2 µm in thickness, while Hy-$NiTiO_3$ nanorods are 2,2 ± 0,9 µm in length and 0,7 ± 0,35 µm thickness.

Figure 3a shows the diffuse reflectance spectra of $NiTiO_3$ samples. This green semiconductor material absorbs in the visible region.

Electrodes based on these nanorods were prepared on FTO and characterized by cyclic voltammetry in the dark. As shown in Figure 3b, the electrochemical response is characterized in both cases by the presence of capacitive currents at potentials more negative than -1 V, as expected for an n-type semiconductor. This capacitive region can be physically associated to the filling with electrons of the conduction band and/or a trap distribution below it. As this accumulation process is accompanied by the insertion/adsorption of cations from the electrolyte, the charge in this region can be considered as a direct measurement of the interfacial area of the electrode (Berger et al., 2012).

The charge accumulation region is slightly larger for the Sono-$NiTiO_3$ sample than for the Hy-$NiTiO_3$. This result agrees well with the fact that the electrodes have approximately the same thickness (Sono-$NiTiO_3$ 2.7 µm, Hy-$NiTiO_3$ 3.2 µm) but the Sono-$NiTiO_3$ is composed by smaller nanorods.

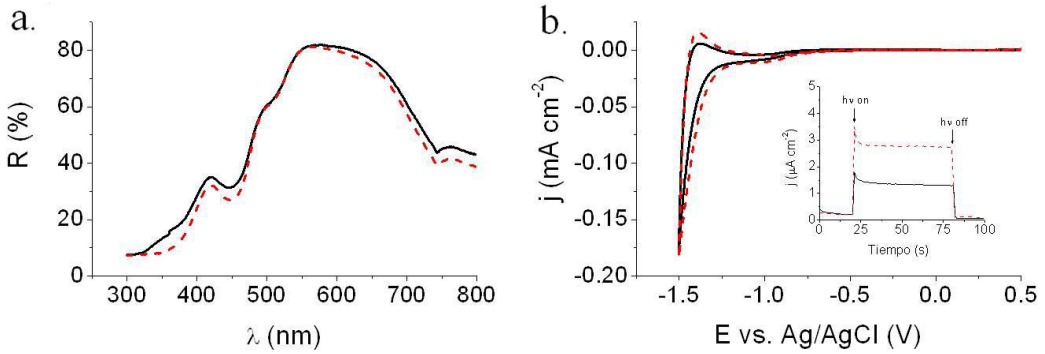

Fig. 3 UV-visible diffuse reflectance spectra (a) and cyclic voltammetry in N_2-purged 1 M NaOH (20 mV/s) (b) for Hy-$NiTiO_3$ (solid line) and Sono-$NiTiO_3$ (dash line). Inset: photocurrent transient at 0.4 V vs. Ag/AgCl.

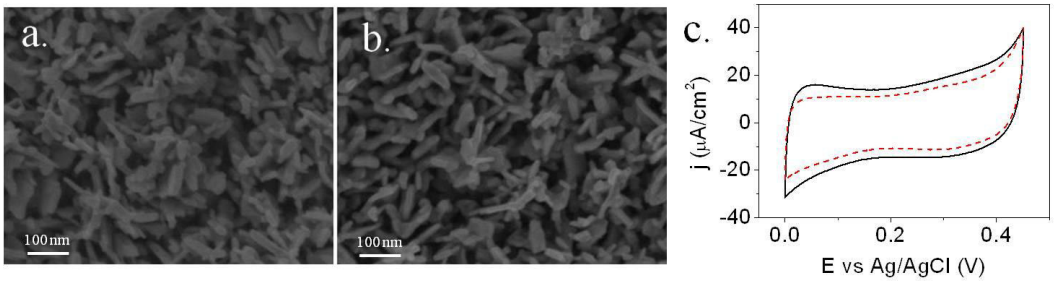

Fig. 4. FE-SEM micrographs of the manganese oxide/FTO electrodes (a) Hy-MnO_x and (b) Sono-MnO_x. Cyclic voltammetry in 0.1 M NaOH (5 mV/s) for Hy-MnO_x (black solid line) and Sono-MnO_x (red dash line) (c).

We have performed some preliminary experiments to verify the possibility of using these materials to perform water photooxidation under white light illumination. At sufficiently positive potentials, a small photocurrent was measured for both samples (inset of Figure 3b). In any case, the electrodes based on the Sono-$NiTiO_3$ nanoparticles were more active. This could be related to the higher interfacial area. Ongoing experiments in our laboratory with these nanomaterials indicate that they can be used for water photooxidation as their properties can be improved by applying appropriate electrochemical pretreatments.

3.3 Synthesis of MnO_x thin films

The preparation of thin films by electrodeposition can be affected by mass transport limitations. Therefore, its combination with ultrasound could be a promising hybrid methodology to prepare thicker films with a better controlled nanostructure. Figure 4 shows the FE-SEM images of the as-prepared MnO_x thin films. No clear differences were observed in the deposit morphology. This agrees with the virtually identical visual aspect of the electrodes and their UV-visible spectra.

As mentioned above, the capacitive currents measured by cyclic voltammetry are directly proportional to the interfacial area of the electrodes. Figure 4c shows the behavior for both electrodes Hy-MnO_x and Sono-MnO_x. The

result points to a very limited effect of sonication during electrodeposition of MnO_x, as the current densities are very similar, implying that not only the same nanostructure is generated, but also the same film thickness is obtained.

3.4 Other results

It is important to highlight that, for some particular preparation routes, the use of even low frequency ultrasound irradiation causes important differences in the final nanostructure. This is the case of the anodization procedures where an improved growth of the as-generated nanotubes (González et al., 2012, Neupane et al., 2013, Zhang et al., 2011) has been reported. In this case, the main effect of the ultrasound field is related with a mass transport improvement that allows for the regeneration of the electrolyte at the electrode-solution interface. In fact, in the absence of ultrasound, usually an amorphous oxo-hydroxide overlayer is generated blocking the entrance of the nanotubes. We have demonstrated that this overlayer on top of the nanotubes can be easily eliminated by ultrasound irradiation, giving rise to the desired open structure (Jankulovska et al., 2013).

4. Conclusions

From these results, we can conclude that the effects of ultrasonic irradiation during the synthesis of oxide nanomaterials are highly dependent on the particular procedure employed. According to the results presented here, ultrasound may influence the final nanoparticle size (as in the case of $NiTiO_3$ nanorods) or the final nanostructure (as in the case of anodization procedures). However, for other synthetic routes the effect is minor or even negligible (as in the case of N-doped TiO_2 nanoparticles, or electrodeposited MnO_x thin films). We believe that ultrasound irradiation can play a key role during the synthesis of metal oxides in those cases where mass transport is highly hindered (as in the case of anodization) and in those procedures that require the rupture of nanoparticle aggregates to obtain a homogenous dispersion.

Acknowledgements

We want to acknowledge the Spanish Ministry of Economy and Competitiveness (MINECO) for financial support through projects PRI-PIBIN-2011-0816 and MAT2012-37676 (FONDOS FEDER). V. Manzi-Orezzoli is grateful to the Universitat d'Alacant for the award of a research initiation grant.

References

A. Gedanken, Ultrasonics Sonochem. 11 (2004) 47.
H. Xu, B.W. Zeiger and K.S. Suslick, Chem. Soc. Rev. 42 (2013) 2555.
H.-Q. Wang, J.-P. Yan, Z.-M. Zhang and W.-F. Chang, React. Kinet. and Catal. Lett. 97 (2009) 91.
J. Geng, L. Jiang and J. Zhu, Sci. China Chem. 55 (2012) 2292.
J. González-García, V. Sáez, I. Tudela, I.M. Díez-García, M.D. Esclapez and O. Louisnard, Water, 2 (2010) 28.
J. H. Bang and K.S. Suslick, Adv. Mater. 22 (2010) 1039.
J. R. González, R. Alcántara, F. Nacimiento, G. F. Ortiz, J. L. Tirado, E. Zhecheva and R. Stoyanova, J. Phys. Chem. C 116 (2012) 20182.
M. Jankulovska, I. Barceló, T. Lana-Villarreal and R.Gómez, J. Phys. Chem. C 117 (2013) 4024.
M. P. Neupane, I. S. Park, T. S. Bae and M. H. Lee, J. Alloys Compd. 581 (2013) 418.
R. Zhang, K. Jiang, Y. Zhu, H. Qi and G. Ding, Appl. Surf. Sci. 258 (2011) 586.
T. Berger, D. Monllor-Satoca, M. Jankulovska, T. Lana-Villarreal and R. Gómez, Chem. Phys. Chem. 13 (2012) 2824.
X.-K. Wang, C. Wang, W.-L. Guo and J.-G. Wang, Material Research Bulletin 46 (2011) 2041.
Y. Gorlin and T. F. Jaramillo, J. Am. Chem. Soc. 132 (2010) 13612.
Y. Qu, W. Zhou, Z. Ren, S. Du, X. Meng, G. Tian, K. Pan, G. Wang and H. Fu, J. Mater. Chem. 22 (2012) 16471.